

Endothelial PI3K-C2 α , a class II PI3K, has an essential role in angiogenesis and vascular barrier function

メタデータ	言語: eng 出版者: 公開日: 2017-10-03 キーワード (Ja): キーワード (En): 作成者: メールアドレス: 所属:
URL	http://hdl.handle.net/2297/32825

Endothelial PI3K-C2 α , a class II PI3K, has an essential role in angiogenesis and vascular barrier function

Kazuaki Yoshioka^{1*}, Kotaro Yoshida^{1,2*}, Hong Cui¹, Tomohiko Wakayama³, Noriko Takuwa^{1,4}, Yasuo Okamoto¹, Wa Du¹, Xun Qi¹, Ken Asanuma⁵, Kazushi Sugihara⁷, Sho Aki¹, Hidekazu Miyazawa¹, Kuntal Biswas¹, Chisa Nagakura¹, Masaya Ueno⁸, Shoichi Iseki³, Robert J. Schwartz⁹, Hiroshi Okamoto¹⁰, Takehiko Sasaki^{5,6}, Osamu Matsui², Masahide Asano⁷, Ralf H. Adams¹¹, Nobuyuki Takakura⁸, and Yoh Takuwa^{1§}

¹Department of Physiology, ²Department of Radiology, and ³Department of Histology and Embryology, Kanazawa University School of Medicine, Kanazawa, Japan, ⁴Department of Health and Medical Sciences, Ishikawa Prefectural Nursing University, Kahoku, Japan, ⁵Department of Medical Biology, Akita University Graduate School of Medicine, ⁶Research Center for Biosignal, Akita University, Akita, Japan, ⁷Division of Transgenic Animal Science, Advanced Science Research Center, Kanazawa University, Kanazawa, Japan, ⁸Department of Signal Transduction, Research Institute for Microbial Diseases, Osaka University, Osaka, Japan, ⁹Department of Biology and Biochemistry, University of Houston, Houston, USA, ¹⁰Department of Medical Biochemistry, Tohoku University School of Medicine, Sendai, Japan, and ¹¹Max Planck Institute for Molecular Biomedicine, Department of Tissue Morphogenesis, and University of Muenster, Faculty of Medicine, Muenster, Germany.

[§]Corresponding author: Yoh Takuwa, M.D., Ph.D., Department of Physiology, Kanazawa University School of Medicine, 13-1 Takara-machi, Kanazawa, 920-8640, Japan, TEL: +81-76-265-2165, FAX: +81-76-234-4223, e-mail: ytakuwa@med.kanazawa-u.ac.jp

* These authors contributed equally to this work.

ABSTRACT

Class II α -isoform of phosphatidylinositol 3-kinases (PI3K-C2 α) is localized in endosomes, the *trans*-Golgi network and clathrin-coated vesicles, however, its functional role is little understood. Global or endothelial cell (EC)-specific targeted disruption of PI3K-C2 α resulted in embryonic lethality due to defects in sprouting angiogenesis and vascular maturation. PI3K-C2 α knockdown in ECs induced decreased phosphatidylinositol 3-phosphate-enriched endosomes, impaired endosomal trafficking, and defective delivery of VE-cadherin to EC junctions and its assembly. PI3K-C2 α knockdown also impeded cell signaling including vascular endothelial growth factor receptor internalization and endosomal RhoA activation. These together led to defective EC migration, proliferation, tube formation and barrier integrity. Endothelial PI3K-C2 α deletion suppressed post-ischemic and tumor angiogenesis, and diminished vascular barrier function, with greatly augmented susceptibility to anaphylaxis and a higher incidence of dissecting aortic aneurysm formation in response to angiotensin II infusion. Thus, PI3K-C2 α plays a crucial role in vascular formation and barrier integrity, and represents a new therapeutic target for vascular diseases.

Formation of the vascular network by vasculogenesis and angiogenesis is essential for embryonic development, repair and remodeling of tissues in adults, as well as tumor growth. The angiogenic response to vascular endothelial growth factor (VEGF) and other factors begins with vascular leakage and dissolution of the subendothelial basement membrane, followed by proliferation and migration of vascular EC^{1,2}. Then, formation of the intercellular junctions results in initial sprouts from existing vessels. The newly formed endothelial tubes are associated with mural cells, *i.e.* smooth muscle cells (SMC) and pericytes, thus becoming mature and stabilized³. Tightness of the intercellular junctions, particularly adherens junctions composed of VE-cadherin, controls vascular permeability^{4,5}. Quiescent, stabilized vasculature with intact barrier integrity dominates in the healthy condition. In contrast, in pathological conditions, such as tumors, the vasculature is generally immature and leaky. In the case of vascular insult such as excessive angiotensin II (Ang II) activity, increased vascular permeability is associated with leukocyte infiltration in the vascular wall and vascular disruption^{6,7}. Therefore, stabilization of the vasculature and maintenance of vascular integrity is essential for vascular and tissue homeostasis^{8,9}.

PI3Ks are an enzyme family that phosphorylates membrane inositol lipids at the 3' position of the inositol ring. The lipid products of PI3Ks serve as important intracellular messengers by interacting with effector proteins, which include protein kinases, guanine nucleotide exchangers for G proteins, and actin cytoskeleton-regulating proteins. Through these actions, PI3Ks regulate a diverse array of cellular processes¹⁰⁻¹². PI3Ks comprise three classes. Class I PI3Ks, which are activated by tyrosine kinases and G protein-coupled receptors, consist of four catalytic subunits: p110 α , p110 β , p110 γ and p110 δ , and mainly produce phosphatidylinositol (PtdIns) 3,4,5-trisphosphates (PtdIns(3,4,5)P₃). Class I PI3Ks, especially p110 α , in EC are indispensable for angiogenesis in the early embryo by regulating EC proliferation, migration and morphogenesis^{13,14}. Class III has a single member, Vps34, which generates PtdIns(3)P to regulate vesicular trafficking¹⁵. In contrast to class I and III, the physiological functions of class II PI3Ks are little understood. Class II PI3Ks comprise three members, PI3K-C2 α (C2 α), PI3K-C2 β (C2 β) and PI3K-C2 γ (C2 γ), and mainly produce PtdIns(3)P *in vivo*^{16,17}. Among the three class II PI3Ks, C2 α is distinct from C2 β , C2 γ and other PI3K

members in that it has unique structures including a clathrin-binding site in the N-terminal stretch and relative resistance to PI3K inhibitors^{16,18}. C2 α is expressed in selected cell populations including epithelium, vascular endothelium, and smooth muscle^{19,20}. C2 α is enriched in clathrin-coated endocytic vesicles, other endosomes and the *trans*-Golgi network (TGN), and is suggested to regulate intracellular vesicular trafficking^{16,18,21,22}. *In vitro* studies^{21,23,24} showed that various extracellular stimuli including cytokines, insulin and integrin ligation modestly stimulated C2 α . However, the *in vivo* function of C2 α is largely unknown, although a recent study²⁵ showed that a hypomorphic C2 α mutant allele resulted in impairment of renal glomerular formation.

By utilizing a gene-targeting strategy, we explored the *in vivo* role of C2 α . We found that C2 α plays a crucial role in developmental and pathological angiogenesis in an EC-autonomous manner. Notably, the angiogenic effect of C2 α is mediated through mechanisms distinct from those of class I PI3Ks: C2 α primarily regulates vesicular trafficking, which is essential for normal delivery of membrane proteins including VE-cadherin and particular cellular signaling, thus playing a pivotal role in EC proliferation, survival, migration, morphogenesis, and thereby angiogenesis. The second crucial role of C2 α in the vasculature is to maintain endothelial barrier function and to protect the vasculature from damage, thus being essential for vascular integrity.

RESULTS

Endothelial C2 α is crucial for developmental and postnatal physiological angiogenesis and vascular maturation

Homozygous global C2 α -deleted mutant (*Pik3c2a*^{-/-}) embryos were growth-retarded from embryonic day 8.5 (E8.5) and died around E10.5–E11.5 due to defects in vascular formation (**Fig. 1, Supplementary Table 1 and Supplementary Figs. 1–3**), suggesting an essential non-redundant role of class II PI3Ks in murine development. Whole-mount CD31 staining of embryos revealed severe defects in vascular development throughout the embryonic body (**Fig. 1a**). In contrast to wild-type (*Pik3c2a*^{+/+}) embryos, the major vessels including the dorsal aorta, intersomitic vessels, and branchial arches were severely disorganized or absent in *Pik3c2a*^{-/-} embryos (*arrowheads in Fig. 1a* (bottom)). Smooth muscle α -actin (α SMA)-positive mural cells were barely detected in the *Pik3c2a*^{-/-} dorsal aorta, but readily detected in heart of *Pik3c2a*^{-/-} as well as wild-type embryos (**Fig. 1b**). In support of the above data, C2 α was highly expressed in vascular EC at the mid-gestation among other cell types including SMC, cardiomyocytes (CM), and gastrointestinal epithelium (**Supplementary Fig. 4**).

To determine the cell type(s) responsible for the phenotype in *Pik3c2a*^{-/-} embryos, three cardiovascular-specific C2 α deletion mutants were generated (**Supplementary Fig. 5**). Both SMC-specific (*Pik3c2a*^{flox/flox}; *SM22 α Cre* = *Pik3c2a* ^{Δ SMC}) and CM-specific (*Pik3c2a*^{flox/flox}; *Nkx2-5Cre*²⁶ = *Pik3c2a* ^{Δ CM}) C2 α -deletion mutants developed normally, and were born with the expected Mendelian ratio (**Supplementary Tables 2 & 3**). However, EC-specific C2 α -deletion mutants (*Pik3c2a*^{flox/flox}; *Tie2Cre*²⁷ = *Pik3c2a* ^{Δ EC}) were embryonic lethal (**Supplementary Tables 3–7**) due to multi-organ abnormalities including severely impaired vascular formation, indicating that endothelial C2 α is essential for normal vascular formation and development. The most severely affected *Pik3c2a* ^{Δ EC} mutants died at E12.5 and phenocopied a global *Pik3c2a*-null embryo. *Pik3c2a* ^{Δ EC} embryos displayed marked dilation of subcutaneous microvessels, with hemorrhage (**Fig. 1c** (bottom)). Double immunofluorescent staining using CD31- and α SMA-specific antibodies of *Pik3c2a* ^{Δ EC} embryo tissue showed decreases in vascular

branching and EC-covered area (31% and 36% reduction, respectively, compared with control embryos. $P < 0.05$, **Fig. 1c,d**), and discontinuous and incomplete coverage of microvessels with vascular SMC (**Fig. 1c** and **Supplementary Fig. 6 a,b**).

Immunostaining using VE-cadherin- and NG2-specific antibodies revealed that the capillaries had discontinuous adherens junction formation and poor coverage with NG2-positive pericytes, which were frequently rounded with cellular processes detached from the capillary wall (**Fig. 1c** and **Supplementary Fig. 6c**). In *Pik3c2a*^{ΔEC};*Rosa26R* embryos, β-galactosidase (βGal)-positive but CD31-negative cord-like cell clusters were interspersed within capillaries (**Fig. 1e** (bottom)). Taken together, these results imply that loss of *C2a* expression in EC is responsible for the phenotype observed in *Pik3c2a*^{-/-} mice.

Since *Pik3c2a*^{ΔEC} (*Pik3c2a*^{flox/flox};*Tie2Cre*) mice are embryonic lethal, we created tamoxifen-inducible, conditional EC-specific *C2α*-deletion mice (*Pik3c2a*^{iΔEC}) which express tamoxifen-activated Cre recombinase under the VE-cadherin promoter²⁸ (*Pik3c2a*^{flox/flox};*Cdh5*(PAC)-CreER^{T2}, **Supplementary Fig. 5e**) and studied the role of *C2α* in postnatal physiological angiogenesis, using a retinal angiogenesis model. Administration of tamoxifen at 3 days after birth (P3) resulted in a marked reduction in *C2α* protein expression at P6 in EC isolated from the lung but not in SMC (**Fig. 2a**). In the retina of mice at P6, EC-specific *C2α* inactivation induced by tamoxifen administration markedly inhibited retinal angiogenesis: the vessel area, the tip cell number and the filopodial number at the vascularizing front was reduced by 46%, 32%, and 48%, respectively, in the superficial layer of the retina in *Pik3c2a*^{iΔEC} mice compared with control mice (**Fig. 2b** and **Supplementary Fig. 7**). Perpendicular sprouting and horizontal network formation in the deeper retina were also severely impaired in the *Pik3c2a*^{iΔEC} retina (**Fig. 2c**). In the retina of *Pik3c2a*^{ΔEC} mice, a marked increase (5.5-fold increase) in apoptosis was observed compared with that in control littermates ($P < 0.01$, **Fig. 2b** (right)). EC-specific hemizygously *C2α*-deleted (*Pik3c2a*^{flox/+};*Tie2Cre*) mice also showed decreased retinal angiogenesis with reduced tip cells and filopodia at the vascularizing front and inhibition of EC proliferation (**Supplementary Fig. 8**).

C2 α is involved in endothelial migration, proliferation and tube-formation through mechanisms involving RhoA regulation

Knockdown of either p110 α or C2 α in human umbilical vein EC (HUVEC) by specific short interfering RNAs (siRNAs), but not by scrambled (sc), C2 β -, Vps34-, or p110 β -specific siRNAs, inhibited VEGF-A-induced capillary-like tube formation (**Fig. 3a** and **Supplementary Fig. 9a,b**). In complete growth medium with serum and growth factor supplements (EBM2TM), knockdown of C2 α still inhibited tube formation whereas knockdown of p110 α or other PI3Ks was ineffective; knockdown of both p110 α and p110 β inhibited tube formation in EBM2 (**Supplementary Fig. 9c**).

C2 α knockdown also markedly inhibited transwell migration of HUVEC toward VEGF-A ($P < 0.001$, **Fig. 3b**) but not of SMC toward PDGF-BB, augmented apoptosis of HUVEC (**Supplementary Fig. 9d,e**) and modestly inhibited serum-induced proliferation (**Supplementary Fig. 9f**). In contrast, C2 α deletion had no effect on proliferation of SMCs (**Supplementary Fig. 9g,h**). These results indicate C2 α -specific, essential roles in EC activities.

C2 α silencing did not alter VEGF-A-induced phosphorylation of VEGF receptor 2 (VEGFR2), p42/p44 ERK, Akt, endothelial NOS (eNOS), or p21-activated kinase-2 (PAK2) (**Fig. 3c**), which differed from the effects of p110 α knockdown¹⁰⁻¹³. However, C2 α knockdown markedly inhibited VEGF-A-induced phosphorylation of MYPT1, a substrate of Rho kinase (**Fig. 3c,d**), and RhoA activation (**Fig. 3e,f**). Consistent with this, immunostaining using an antibody that specifically recognizes the GTP-bound active form of RhoA (**Supplementary Fig. 10a**) showed that knockdown of either C2 α or p110 α suppressed VEGF-A-induced RhoA activation (**Supplementary Fig. 10b**). Knockdown of C2 α but not of p110 α or Vps34 inhibited serum/growth factor supplements-induced RhoA activation (**Supplementary Fig. 10c**). C2 α knockdown also reduced VEGF-A-induced Rac1 and FGF2-induced Rap1 activation (**Supplementary Fig. 11**), which participate in stabilizing VE-cadherin at EC-EC contacts^{5,29}.

RhoA knockdown, as well as VE-cadherin knockdown, abolished VEGF-A-induced tube formation ($P < 0.01$, **Supplementary Fig. 12a,b**). In a mixed culture of dominant negative RhoA mutant RhoA^{N19}-expressing HUVEC and control HUVEC, RhoA^{N19}-

expressing HUVEC showed rounded cells that failed to form cell-cell contacts through cell protrusions as seen in normal HUVEC (**Supplementary Fig. 12c,d** (*red arrowheads* in right panel)). These observations together suggest that C2 α plays an essential role for morphogenesis through the mechanisms involving RhoA.

C2 α is required for endosomal trafficking, which is crucial for Rho-dependent VE-cadherin delivery and assembly

In sc-siRNA-treated control HUVEC that were transfected with the PtdIns(3)P-specific probe mRFP-tagged 2 \times FYVE domain^{30,31}, the mRFP-2 \times FYVE signal was mainly localized in endosomes (**Fig. 4a**). C2 α depletion markedly reduced the number of mRFP-2 \times FYVE⁺-vesicles ($P < 0.01$), whereas PI3K p110 α - or Vps34-depletion did not alter the number of mRFP-2 \times FYVE⁺-vesicles. Total cellular content of PtdIns(3)P, but not PtdIns(3,4)P₂, PtdIns(3,5)P₂ and PtdIns(3,4,5)P₃, in C2 α -deleted cells was reduced compared with that in control cells (**Supplementary Fig. 13**). Thus, C2 α has a significant contribution to PtdIns(3)P accumulation in the endosomal compartment. Consistent with this, C2 α was detected in a granular pattern in HUVEC with enrichment in the perinuclear region, and partially co-localized with markers of clathrin-coated vesicles, TGN and early endosomes (**Supplementary Fig. 14a–c**)^{16,18,22}. GFP-C2 α also substantially overlapped with mRFP-2 \times FYVE (**Supplementary Fig. 15a** and **Movie 1**). The motility, fusion and fission of GFP-2 \times FYVE⁺-vesicles were markedly attenuated in C2 α -depleted cells (**Supplementary Movies 2 & 3**), suggesting that C2 α is involved in endosomal trafficking. Knockdown of C2 α , but not of p110 α or Vps34, caused enlargement of the Golgi/TGN area (**Supplementary Fig. 14d**). Swelling of the Golgi/TGN compartment was also demonstrated in EC of the *Pik3c2a*^{-/-} dorsal aorta by electron microscopy (**Supplementary Fig. 14e**).

In C2 α -depleted, but not p110 α - or Vps34-depleted, EC, the trafficking of VE-cadherin between the TGN and the intercellular junctions at the plasma membrane was disrupted (**Fig. 4b** and **Supplementary Movies 4 & 5**). C2 α was partially co-localized with VE-cadherin in the Golgi/TGN and endosomes but not in the intercellular junction (**Supplementary Fig. 15b**). A portion of mRFP-2 \times FYVE⁺-vesicles were positive for VE-cadherin-GFP, suggesting the transport of VE-cadherin by PtdIns(3)P⁺-vesicles

(**Supplementary Fig. 15c**). In agreement with these findings, the accumulation of VE-cadherin at the cell-cell contacts in C2 α -depleted, but not p110 α - or Vps34-depleted, HUVEC was reduced and discontinuous, with reduced β -catenin association and intracellular instability of VE-cadherin protein compared with that in control HUVEC (**Fig. 4c** and **Supplementary Fig. 16a,b**). Expression of RhoA^{N19} impaired VE-cadherin trafficking between the TGN and the plasma membrane, thereby resulting in disturbed VE-cadherin clustering at cell-cell contacts (**Fig. 4b** (bottom), **Supplementary Movie 6**, and **Supplementary Fig. 16c**). In mixed cultures of normal HUVEC and RhoA-depleted HUVEC, VE-cadherin clustering was impaired at the boundary between RhoA-depleted cells (**Supplementary Fig. 16d**). In C2 α -depleted HUVEC, the expression of the constitutively active RhoA mutant GFP-RhoA^{V14} but not of GFP-wild-type RhoA partially restored defective VE-cadherin clustering at the cell-cell contacts (*arrowheads* in **Supplementary Fig. 16e**), whereas in sc-siRNA-treated control HUVEC the expression of GFP-RhoA^{N19} but not of GFP-wild-type RhoA attenuated VE-cadherin assembly.

Because C2 α is necessary for endosomal trafficking and endosomes are now recognized to be involved in the activation of signaling molecules including Rho GTPases³², we explored how C2 α regulates RhoA activation in cells by adopting a fluorescence resonance energy transfer (FRET) imaging technique. RhoA was activated in both the intracellular vesicular compartment and the plasma membrane, with intense signals at cell-cell contacts in HUVEC (**Fig. 4d**, **Supplementary Movie 7**). A substantial portion of the intracellular FRET signal coincided with 2 \times FYVE signals (**Fig. 4e**). C2 α knockdown inhibited the RhoA-FRET signal in both the endosomes and the plasma membrane (**Fig. 4d–g**, **Supplementary Movie 8**), indicating that C2 α is necessary for RhoA activation in PtdIns(3)P-enriched endosomes and the plasma membrane. We further studied the role of C2 α in VEGF receptor internalization, which could be an event upstream of RhoA activation. VEGF-A stimulated the internalization of VEGFR2 into the 2 \times FYVE⁺-vesicular compartment (**Fig. 4h**, **left**), which was dampened by C2 α depletion (**Fig. 4h**, **right**). VEGF-A stimulation induced phosphorylation of VEGFR2 at the plasma membrane in HUVEC at 2 min, and most phosphorylated VEGFR2 was re-distributed in the intracellular compartment, mainly in EEA1⁺-endosomes, at 30 min

(**Supplementary Fig. 17** (upper)). C2 α depletion did not inhibit the initial VEGFR2 phosphorylation in the plasma membrane at the early time point but inhibited the internalization of phosphorylated VEGFR2 (**Supplementary Fig. 17** (lower)). Furthermore, dynasore, an inhibitor of dynamin-dependent endocytosis³³, inhibited growth factor-induced RhoA activation, VE-cadherin assembly and tube formation (**Supplementary Fig. 18a–d**). Thus, C2 α is indispensable for internalization of activated receptors, activation of RhoA and other signaling molecules on endosomes, RhoA-dependent trafficking and assembly of VE-cadherin, and endothelial morphogenesis.

Endothelial C2 α is essential for post-ischemic and tumor angiogenesis

We studied the role of endothelial C2 α in pathological angiogenesis using post-ischemic and tumor angiogenesis models. In *Pik3c2a*^{iAEC} mice, the recovery of blood flow in the ischemic hindlimb after surgical femoral arteriectomy was suppressed during the postoperative days 14–28 compared with that in control *Pik3c2a*^{flox/flox} mice ($P < 0.0001$ on day 28, **Fig. 5a**). Immunofluorescent staining using CD31-specific antibody showed an approximately 50% decrease in microvessels in ischemic muscle of *Pik3c2a*^{iAEC} mice on postoperative day 28 ($P < 0.0001$, **Fig. 5b**). *Pik3c2a*^{iAEC} mice exhibited diminished tumor volumes and weight of implanted Lewis lung carcinoma (LLC) and B16-BL6 melanoma tumor compared with control *Pik3c2a*^{flox/flox} mice ($P < 0.01$, **Fig. 5c**). Immunofluorescent staining using CD31-specific antibody showed that the microvessel density in LLC tumors was reduced in *Pik3c2a*^{iAEC} mice compared with that in control mice ($P < 0.05$, **Fig. 5d**). Moreover, double-immunostaining with CD31- and NG2-specific antibodies revealed that the tumor microvessels in *Pik3c2a*^{iAEC} mice had poor coverage with NG2⁺-pericytes, which were frequently rounded or detached from the microvessels (**Fig. 5e**).

C2 α is required for vascular barrier function and integrity

The permeability of a monolayer of C2 α -depleted HUVEC was increased under both resting and VEGF-A-stimulated conditions compared with that of control HUVEC ($P < 0.05$, **Fig. 6a**). VEGF-A induced a greater increase in leakage of intravenously administered Evans blue dye in the skin of *Pik3c2a*^{+/-} mice ($P < 0.05$, **Fig. 6b**). We

studied the vascular responses to hyperpermeability- and inflammation-eliciting insults in global *Pik3c2a*^{+/-} and wild-type mice. Intravenous (*i.v.*) injection of a low-dose of platelet-activating factor (PAF), a mediator of anaphylactic shock³⁴, did not affect survival in wild-type mice whereas it induced death in all *Pik3c2a*^{+/-} littermates within 40 min with increases in hematocrit and Evans blue leakage in the lung (**Fig. 6c,d**). A higher dose of PAF, which induced death only in a portion (about 30%) of wild-type mice, caused more rapid death of all *Pik3c2a*^{+/-} mice. PAF-induced increases in plasma histamine and IL-4, anaphylactic mediators, were similar in wild-type and *C2α*^{+/-} mice (**Supplementary Fig. 19**), suggesting that *C2α* deficiency primarily impairs endothelial function, resulting in vascular barrier disruption.

In *Pik3c2a*^{+/-} mice, chronic Ang II infusion induced more robust hyperpermeability in the aorta and coronary vessels compared with that in wild-type littermates (**Fig. 6e**). *En face* immunostaining using VE-cadherin-specific antibody of the aorta showed disorganization of adherens junctions in *Pik3c2a*^{+/-} mice given Ang II (**Fig. 6f**). Concomitantly, a higher incidence of aortic aneurysms with dissection, resultant rupture and death was observed in *Pik3c2a*^{+/-} mice compared with wild-type littermates (aneurysm occurrence; 23/48 *Pik3c2a*^{+/-} mice vs. 5/44 wild-type mice) ($P < 0.01$, **Fig. 6g & h**). Conditional EC-specific deletion of *C2α* also resulted in a higher occurrence of dissecting aneurysms compared with control mice (aneurysm occurrence; 5/20 *Pik3c2a*^{iΔEC} mice vs. 1/13 control mice) ($P < 0.01$, **Fig. 6g**). There was no difference in blood pressure between *Pik3c2a*-deleted and control mice (data not shown). Thus, the aortic wall of *C2α*-deficient mice seems to be fragile compared with that of WT mice. AngII infusion stimulated MMP-2 and MMP-9 activities, which are implicated in the formation of aneurysms^{6,7,35,36}, in the aortic tissue, with a greater increase in *Pik3c2a*^{+/-} mice compared with wild-type mice ($P < 0.05$, **Fig. 6i**). Immunostaining using Mac3-specific antibody, a macrophage marker, revealed a greater number of infiltrating macrophages, which are the major source of MMPs, mainly in the adventitia of *Pik3c2a*^{+/-} mice compared with wild-type mice (**Fig. 6j**).

DISCUSSION

This study shows that the class II PI3K-C2 α in EC has indispensable roles in sprouting angiogenesis and subsequent mural cell recruitment, and in maintaining vascular barrier integrity in quiescent vessels. Deficient C2 α actions result in impaired angiogenesis and pathological vascular hyperpermeability with vascular damage. At the cellular level, C2 α is essential for EC migration, proliferation/survival and VE-cadherin assembly at the intercellular junction. The actions of C2 α are mediated by its regulatory effects on the intracellular vesicular transport, *i.e.* the delivery and recycling of membrane molecules, and cell signaling, which likely occurs on endosomes (**Supplementary Fig. 20**). These C2 α actions underlie its roles in angiogenesis and barrier integrity. The actions of C2 α and class I PI3Ks in EC are distinct in that, different from C2 α , class I PI3Ks exert a great impact on Akt stimulation and cell proliferation and are not involved in vesicular trafficking including VE-cadherin transfer or VE-cadherin assembly at the cell-cell junction¹⁰⁻¹³. Therefore, these observations reveal novel biological activities of C2 α and underscore broader roles for PI3K family members in vascular physiology and pathophysiology.

In contrast to class I PI3Ks that generate PtdIns(3,4,5)P₃, the major product of class II and III PI3Ks is PtdIns(3)P, which is mainly accumulated in endosomes^{16-18,20-25}. Consistent with this, C2 α in EC was localized in endosomes and TGN, which are organelles responsible for processing, sorting and packaging proteins into distinct carriers for transport to their final destinations. Another class II PI3K-C2 β and class III Vps34 are also localized primarily in the clathrin-coated or endocytic compartment^{38,39}. Localized production of PtdIns(3)P together with Rab GTPases including Rab5 on the endocytic membrane causes the recruitment of proteins such as early endosome antigen 1 (EEA1) and Rabenosyn-5 to facilitate dynamic formation of endocytic membranous structures for uptake, packaging and sorting^{30,39}. In EC, C2 α is an PI3K isoform that is largely responsible for PtdIns(3)P accumulation on endosomes and seems to have a functionally distinct role from those of C2 β and Vps34: depletion of C2 α but not Vps34 severely impairs trafficking of 2 \times FYVE⁺-vesicles. Among others, C2 α deficiency impedes delivery of VE-cadherin to intercellular junctions and its normal assembly. C2 α is also necessary for receptor internalization. Thus, C2 α is likely located in a different endocytic

compartment from C2 β and Vps34 in EC or C2 α activity is regulated differentially from that of C2 β and Vps34^{18,23,40}. Thereby, C2 α serves specialized functions in vesicular trafficking in EC.

Our data also show that C2 α is involved in cell signaling. Endocytosis has long been recognized as a mechanism for terminating signaling by internalizing and degrading cell surface receptors³⁹. Besides this classical role of endocytosis, recent studies^{32,42,43} demonstrate that endosomes serve as platforms to assemble membrane receptors and their downstream signaling molecules and to generate spatially localized signals. In EC, activation of RhoA, Rac1 and Rap1 but not Akt or ERK by VEGF-A and FGF2 is dependent on C2 α to varied extents, indicating that the generation of particular intracellular signals requires C2 α . Our study shows that C2 α is essential for the internalization of activated VEGFR2 and endosomal RhoA activation. Consistent with the role of endosomes in receptor signaling, blockade of endocytosis suppressed VEGF-A-induced RhoA activation. Localized activation of RhoA was recently shown to be necessary for proper assembly of VE-cadherins at the intercellular junctions and a barrier-protective activity⁴⁴⁻⁴⁶, although evidence for the opposite barrier-disruptive activity of RhoA has accumulated^{4,47}. Our data indicate that C2 α -dependent RhoA activity on endosomes is crucial for delivery and assembly of VE-cadherin at the cell boundary and cell-cell contact formation. The Rho-guanine nucleotide exchange factor (Rho-GEF), which is responsible for VEGF-induced endosomal RhoA activation in EC, and the molecular mechanisms for recruitment and activation of the Rho-GEF remain to be determined. Rap1 and Rac1 are also implicated in strengthening the VE-cadherin-mediated intercellular junction^{4,48,49}.

The present study suggests that the effects of C2 α on endocytic trafficking play a pivotal role in EC migration, proliferation/survival and vascular morphogenesis through endosomal transport and signaling. For example, Rho and Rac are activated at the rear and front ends, respectively, in migrating cells to drive machineries to retract the rear portion of the cell body and to extend protrusions forward. During cell migration, there is assembly and disassembly of focal adhesions, which is carried out by endocytic and recycling vesicular movements^{49,50}. Rho GTPases are involved in the formation of focal adhesions. Focal adhesions also serve as signaling machinery to generate cell survival

signals through mechanisms involving integrin ligation. Polarization of the EC monolayer in the vascular wall also depends on membrane trafficking⁵¹. Endosomes could be involved in these processes through both serving as a platform for the activation of Rho GTPases and recruiting Rho GTPases to specific sites within cells⁴⁵. Taken together, our observations strongly suggest that C2 α fulfills a role in angiogenesis and vascular integrity through regulating vesicular trafficking.

In adult mice, C2 α expression is generally diminished compared with that in embryos, but is still dominant in the vascular endothelium among other tissues¹⁹. Our data show that C2 α is essential for maintaining barrier integrity in quiescent vessels as evidenced by its protective role against VEGF-A-induced hyperpermeability. In anaphylaxis, a 50% reduction in C2 α expression markedly increased mortality. In chronic vascular injury induced by Ang II infusion, disruption of the vascular wall occurs, leading to fatal dissecting aneurysm formation. C2 α also likely plays a role in maintaining EC survival and vascular stability in quiescent vessels. Collectively, our data are consistent with the notion that a normal level of C2 α expression is essential for the maintenance of vascular integrity in quiescent vasculature as well as in neovessel formation. These observations point to the possibility that C2 α may become a new therapeutic target for vascular diseases caused by barrier disruption.

METHODS

Methods and associated references are available in the online version of the paper at <http://www.nature.com/naturemedicine/>.

Note: Supplementary information is available on the Nature Medicine website.

ACKNOWLEDGMENTS

We thank K. Mitsumori for comments on histological study. We thank N. Mochizuki and K. Ando for assistance of the FRET imaging analysis. We thank N. Furusawa, K. Sunagawa and E. Kaneko for assistance with live-cell imaging using a Yokogawa confocal microscope system. We also thank Y. Ohta and T. Murakawa for technical assistance and T. Hirose for administrative assistance. C2 α cDNA was obtained from J. Domin (Imperial College London). GFP-2 \times FYVE and mRFP-2 \times FYVE expression vectors were obtained from H. Stenmark (Oslo University Hospital) and Y. Ohsumi

(Tokyo Institute of Technology), respectively. VE-cadherin-GFP expression vector were obtained from N. Mochizuki (National Cerebral and Cardiovascular Center). pRaichu-RhoA probe was obtained from M. Matsuda (Kyoto University) GFP-RhoA^{N19} and GFP-RhoA^{V14} expression vectors were obtained from F. Valderrama (King's College London). This work was supported in part by grants-in-aid from the Japanese Ministry of Education, Culture, Sports, Science and Technology, the Japan Society for the Promotion of Science (to K.Yoshioka, N.T., O.Y. and Y.T.), the Honjin Foundation, the Mitsubishi Pharma Research Foundation and the SENSIN Medical Research Foundation (to K.Yoshioka.).

AUTHOR CONTRIBUTIONS

K.Yoshioka the designed the experiments, performed characterization of developmental and retinal angiogenesis of the conditional KO mice and most of the *in vitro* studies, and analyzed the data with assistance from N.Takuwa, Y.O., W.D., S.A., H.M., C.N., M.U., K.B., and O.M. K.A. and T.S. analyzed the cellular content of phosphoinositides. K.Yoshida performed *in vivo* angiogenesis experiments with K.Yoshioka, tumor implantation and aneurysm experiments, and interpreted the results. H.C. performed the anaphylaxis experiments. D.W. performed the *in vivo* permeability study. X.Q. and Y.O. performed and interpreted the results of the ischemic angiogenesis model. T.W. and S.I. performed and interpreted the results of electron microscopy. K.S., M.A., N. Takuwa, R.J.S., H.O., and R.H.A. generated mouse mutants. K.Yoshioka and Y.T. planned and supervised the experiments, arranged the figures and wrote the manuscript. M.A. and N. Takuwa participated in writing the manuscript (M.A.: part of the Methods, N. Takuwa: the Abstract, Introduction and Results in the paper).

COMPETING FINANCIAL INTERESTS

The authors declare no competing financial interests.

REFERENCES

1. Adams, R.H. & Alitalo, K. Molecular regulation of angiogenesis and lymphangiogenesis. *Nature Rev. Mol. Cell Biol.* **11**, 329–341 (2010).
2. Coultas, L. *et al.* Endothelial cells and VEGF in vascular development. *Nature* **438**, 937–945 (2005).
3. Andrae, J. *et al.* Role of platelet-derived growth factor in physiology and medicine. *Genes Dev.* **22**, 1276–1312 (2008).
4. Mehta, D. & Malik, A.B. Signaling mechanisms regulating endothelial permeability. *Physiol. Rev.* **86**, 279–367 (2006).
5. Dejana, E., Tournier-Lasserre, E. & Weinstein B.M. The control of vascular integrity by endothelial cell junctions: Molecular basis and pathological implications. *Dev. Cell* **16**, 209–221 (2009).
6. Yoshimura, K. *et al.* Regression of abdominal aortic aneurysm by inhibition of c-Jun N-terminal kinase. *Nature Med.* **11**, 1330–1338 (2005).
7. Satoh, K. *et al.* Cyclophilin A enhances vascular oxidative stress and the development of angiotensin II-induced aortic aneurysms. *Nature Med.* **15**, 649–656 (2007).
8. Ferrara, N. & Kerbel, R.S. Angiogenesis as a therapeutic target. *Nature* **438**, 967–974 (2005).
9. Carmeliet, P. Angiogenesis in life, disease and medicine. *Nature* **438**, 932–936 (2005).
10. Engelman, J. A. *et al.* The evolution of phosphatidylinositol 3-kinases as regulator of growth and metabolism. *Nature Rev. Genet.* **7**, 606–619 (2006).
11. Takenawa, T. & Suetsugu, S. The WASP-WAVE protein network: connecting the membrane to the cytoskeleton. *Nature Rev. Mol. Cell Biol.* **8**, 37–48 (2007).
12. Vanhaesebroeck, B. *et al.* The emerging mechanisms of isoform-specific PI3K signaling. *Nature Rev. Mol. Cell Biol.* **11**, 329–341 (2010).
13. Graupera, M. *et al.* Angiogenesis selectively requires the p110 α isoform of PI3K to control endothelial cell migration. *Nature* **453**, 662–666 (2008).
14. Yuan, T. & Cantley, L.C. PI3K pathway alterations in cancer: variations on a theme. *Oncogene* **27**, 5497–5510 (2008).
15. Funderburk, S.F., *et al.* The Beclin 1-Vps34 complex at the crossroads of autophagy and beyond. *Trends. Cell Biol.* **20**, 355–362 (2010).
16. Falasca, M. *et al.* The role of phosphoinositide 3-kinase C2 α in insulin signaling. *J. Biol. Chem.* **282**, 28226–28236 (2007).
17. Linassier, C. *et al.* Molecular cloning and biochemical characterization of a Drosophila phosphatidylinositol-specific phosphoinositide 3-kinase. *Biochem. J.* **321**, 849–856 (1998).
18. Domin, J. *et al.* The class II phosphoinositide 3-kinase PI3K-C2 α is concentrated in the trans-Golgi network and present in clathrin-coated vesicles. *J. Biol. Chem.* **275**, 11943–11950 (2000).
19. El Sheikh, S.S., *et al.* Topographical expression of class IA and class II phosphoinositide 3-kinase enzymes in normal human tissues is consistent with a role in differentiation. *BMC Clin. Pathol.* **3**, 1–14 (2003).
20. Yoshioka, K. *et al.* Ca²⁺-induced, Rho- and Rho kinase-dependent regulation of myosin phosphatase and contraction in isolated vascular smooth muscle cells. *Mol. Pharmacol.* **71**, 912–920 (2007).
21. Traer, C.J. *et al.* Are class II phosphoinositide 3-kinases potential targets for anticancer therapies? *Bull Cancer* **93**, E53–8 (2006).

22. Gaidarov, I. *et al.* Individual phosphoinositide 3-kinase C2 α domain activities independently regulate clathrin function. *J. Biol. Chem.* **280**, 40766–40772 (2005).
23. Falasca, M. & Maffucci, T. Role of class II phosphoinositide 3-kinase in cell signalling. *Biochem. Society Transactions* **35**, 211–214 (2006).
24. Wang, Y. *et al.* Class II phosphoinositide 3-kinase α -isoform regulates Rho, myosin phosphatase and contraction in vascular smooth muscle. *Biochem J.* **394**, 581–592 (2006).
25. Harris, D. *et al.* Requirement for class II phosphoinositide 3-kinase C2 α in maintenance of glomerular structure and function. *Mol. Cell. Biol.* **31**, 63–80 (2011).
26. Moses, K.A. *et al.* Embryonic expression of an Nkx2-5/Cre gene using ROSA26 reporter mice. *Genesis.* **31**, 176–180 (2001).
27. Kisanuki Y.Y. *et al.* Tie2-Cre transgenic mice: A new model for endothelial cell-lineage analysis in vivo. *Dev. Biol.* **230**, 230–242 (2001).
28. Wang, Y. *et al.* Ephrin-B2 controls VEGF-induced angiogenesis and lymphangiogenesis. *Nature* **465**, 483–486 (2010).
29. Pannekoek, W. *et al.* Cell-cell junction formation: The role of Rap1 and Rap1 guanine nucleotide exchange factors. *Biochim. Biophys. Acta*, **1788**, 790–796 (2009).
30. Gillooly, D. J. *et al.* Localization of phosphatidylinositol 3-phosphate in yeast and mammalian cells. *EMBO J.* **19**, 4577–4588 (2000).
31. Lindmo, K. & Stenmark, H. Regulation of membrane traffic by phosphoinositide 3-kinase. *J. Cell Sci.* **119**, 605–614 (2006).
32. Di Paolo, G. & De Camilli, P. Phosphoinositides in cell regulation and membrane dynamics. *Nature* **443**, 651–657 (2006).
33. Macia, E. *et al.* Dynasore, a cell-permeable inhibitor of dynamin. *Dev. Cell* **10**, 839–850 (2006)
34. Cauwels, A. *et al.* Anaphylactic shock depends on PI3K and eNOS-derived NO. *J. Clin. Invest.* **116**, 2244–2251 (2006)
35. Daugherty, A. & Cassis L.A. Mouse models of abdominal aortic aneurysms. *Arterioscler Thromb Vasc Biol.* **24**, 429–434 (2004).
36. Di Gennaro, A. *et al.* Increased expression of leukotriene C4 synthase and predominant formation of cysteinyl-leukotrienes in human abdominal aortic aneurysm. *PNAS* **107**, 21093–21097 (2010).
37. Wheeler, M. & Domin, J. The N-terminus of phosphoinositide 3-kinase-C2 β regulates lipid kinase activity and binding to clathrin. *J. Cell. Physiol.* **206**, 586–593 (2006).
38. Simonsen, A. & Tooze, S.A. Coordination of membrane events during autophagy by multiple class III PI3-kinase complexes. *J. Cell Biol.* **186**, 773–782 (2009).
39. Caswell, P. & Norman, J. Endocytic transport of integrins during cell migration and invasion. *Trends Cell Biol.* **18**, 257–263 (2008).
40. Johnson, E.E. *et al.* Gene silencing reveals a specific function of hVps34 phosphatidylinositol 3-kinase in late versus early endosomes. *J. Cell Sci.* **119**, 1219–1232 (2005).
41. Doherty, G.J. & McMahon, H.T. Mechanisms of endocytosis. *Annu. Rev. Biochem.* **78**, 31.1–31.46 (2009)
42. Zoncu, R. *et al.* A phosphoinositide switch controls the maturation and signaling properties of APPL endosomes. *Cell* **136**, 1110–1121 (2009).
43. Palamidessi, A. *et al.* Endocytic trafficking of Rac is required for the spatial restriction of signaling in cell migration. *Cell* **134**, 135–147 (2008).

44. van Nieuw Amerongen, G. P. *et al.* Involvement of Rho kinase in endothelial barrier maintenance. *Arterioscler. Thromb. Vasc. Biol.* **27**, 2332–2339 (2007).
45. Yamada, S. & Nelson, W.J. Localized zones of Rho and Rac activities drive initiation and expansion of epithelial cell-cell adhesion. *J. Cell. Biol.* **178**, 517–527 (2007).
46. Harris, T. J. C. & Tepass, U. Adherens junctions: from molecules to morphogenesis. *Nature Rev. Mol. Cell Biol.* **11**, 502–514 (2010).
47. Abraham, S. *et al.* VE-cadherin-mediated cell-cell interaction suppresses sprouting via signaling to MLC2 phosphorylation. *Curr. Biol.* **19**, 668–674 (2009).
48. Noda, K. *et al.* Vascular endothelial-cadherin stabilizes at cell-cell junctions by anchoring to circumferential actin bundles through α - and β -catenins in cyclic AMP-Epac-Rap1 signal-activated endothelial cells. *Mol. Biol. Cell* **21**, 584–596 (2010).
49. Webb, S.G., Parsons, J.T. & Horwitz, A.F. Adhesion assembly, disassembly and turnover in migrating cells – over and over and over again. *Nat Cell Biol.* **4**, E97–100 (2002).
50. Mitra, S.K., Hanson, D.A. & Schlaepfer, D.D. Focal adhesion kinase: In command and control of cell motility. *Nat Rev. Cell Biol.* **6**, 56–68 (2005).
51. Shivas, J.M. *et al.* Polarity and endocytosis: reciprocal regulation. *Trends Cell Biol.* **20**, 445–452 (2010).

ONLINE METHODS

Mice. All mice used in this study were bred and maintained at Institute for Experimental Animals, Advanced Science Research Center, Kanazawa University, under specific pathogen-free conditions. All procedures were conducted in accordance with Fundamental Guidelines for Proper Conduct of Animal Experiment and Related Activities in Academic Research Institutions under the jurisdiction of the Ministry of Education, Culture, Sports, Science and Technology of Japan approved by the Committee on Animal Experimentation of Kanazawa University.

A gene-targeting strategy to generate global *Pik3c2a*-null mice is described in Supplementary Methods. Four lines of *Cre*-mice, *Tie2Cre*²⁷, *SM22 α Cre* (B6.129S6-*Tagln*^{tm2(cre)^{Yec}}/J, Jackson Lab.), *Nkx2-5Cre*²⁶ and tamoxifen-inducible EC-specific *Cdh5(PAC)-CreER*^{T2} (ref.28,52,53); *Pik3c2a*^{flox/+} mice and *Pik3c2a*^{flox/flox} mice were bred to generate *Pik3c2a* ^{Δ EC} (*Pik3c2a*^{flox/flox}; *Tie2Cre*), *Pik3c2a* ^{Δ SMC} (*Pik3c2a*^{flox/flox}; *SM22 α Cre*), *Pik3c2a* ^{Δ MC} (*Pik3c2a*^{flox/flox}; *Nkx2-5Cre*) and *Pik3c2a* ^{Δ EC} (*Pik3c2a*^{flox/flox}; *Cdh5(PAC)-CreER*^{T2}) mice, respectively. Cre-negative littermates were used as control mice. To verify the efficiency of Cre recombination, Cre mice were mated with animals of the *Cre* reporter transgenic line *ROSA26-LacZ* (B6.129S4-*Gt(ROSA)26Sor*^{tm1Sor}/J, Jackson Lab.). All animals had a C57BL/6J genetic background. Gene inactivation in pups was triggered by intraperitoneal (*i.p.*) injection of 50 μ l of tamoxifen solution (Sigma, T5648; 10 mg ml⁻¹ corn oil) once at P3 or P6. The phenotypes of mutant mice were analyzed at P6 or P9, as indicated. For adult mice, tamoxifen was administered by intraperitoneal (*i.p.*) injection of 100 μ l of a 10 mg ml⁻¹ tamoxifen stock solution (= 1 mg per injection) a total of 7 times, every second day.

Cell culture and siRNA knockdown. Mouse embryonic fibroblasts (MEF) and aortic smooth muscle cells (MASM) were isolated from *Pik3c2a*^{flox/flox} mice and used for *in vitro* assay. *Pik3c2a*^{flox/flox} MEF and MASM cells were cultured in Dulbecco's modified minimal essential medium (DMEM) (WAKO) and advanced DMEM (Invitrogen) supplemented with 10% fetal bovine serum (FBS), respectively, up to 70% confluency and then were infected with adenovirus-encoding cre recombinase (AdCre) in the absence of serum. Infection with adenovirus-encoding LacZ (AdLacZ) was used as control. After 1 h, culture medium containing 10% FBS was added, and cells were allowed to recover for the next 48 h. Greater than 90% C2 α deletion was confirmed by western blotting. HUVEC (passage 2–4) (Lonza) were grown in endothelial basal medium supplemented with 2% FBS and growth factor supplements cocktail (complete growth medium) (EBM2TM; Lonza #CC-3162). HUVEC were transfected with 20 nM of short interfering RNA (siRNA) using Lipofectamine 2000 (Invitrogen) in OptiMEM (2 μ l ml⁻¹, Gibco) according to the manufacturer's instructions. After 4 h, the media were replaced with complete growth medium. The cells were cultured for further 48–72 h before processing for immunofluorescence staining and other assays. Target sequences of siRNA used in this report were listed in *siRNA in Supplementary Methods*.

Whole-mount staining and immunofluorescent staining. For tissue immunohistochemistry, 4% paraformaldehyde (PFA)-fixed, paraffin embedded tissue sections were stained using standard methods. The frozen sections were prepared by cryoprotecting fixed tissue in 20% sucrose for overnight at 4 °C, snap-frozen in Optimal Cutting Temperature (OCT) compound (Tissue Tek) and sectioning with a Sakura Tissue-Tek Cryo₃ Cryostat. Sections (7–30 μm) were washed in Ca²⁺- and Mg²⁺-free Dulbecco's phosphate buffered saline (PBS) and incubated with primary antibodies diluted in the antibody dilution solution (Can Get Signal, Toyobo) overnight at 4 °C or for 2 h at room temperature. Sections were then washed in PBS with 0.1% Triton X-100 and incubated with Alexa Flour-conjugated secondary antibodies for 1 h at room temperature. Antibodies used in this report were listed in *Antibodies and Reagents* in *Supplementary Methods*. Whole-mount immunostaining of CD31 was performed using the labeled streptavidin biotin method as described previously⁵⁴. Alternatively, skin from the embryo head region, flat-mount retinas from postnatal mice (P6 or P9), and *en face* preparations of mouse aorta were used for whole-mount immunostaining, as described previously⁵⁵ with minor modification. PFA-fixed tissues were permeabilized with methanol when necessary. Samples were incubated in blocking buffer (1% BSA, 0.3% Triton X-100 in PBS) for 2 h, washed three times in Pblec buffer (1% Triton X-100, 1 mM CaCl₂, 1 mM MgCl₂, 1 mM MnCl₂ in PBS, pH 6.8), and incubated overnight with biotinylated isolectin B4 (Vector B-1205, 1:50) and CD31- (1:100), FITC-conjugated SMα-actin- (1:100), NG2- (1:100) and biotinylated VE-cadherin- (1:100) specific antibodies diluted in Pblec buffer at 4 °C with gentle rocking. For secondary detection, Alexa Fluor-594-conjugated streptavidin (1:200) or Alexa Fluor-488-conjugated species-specific IgG antibodies (1:500) diluted in blocking buffer were applied overnight at 4 °C.

For immunofluorescent cell staining, cells were cultured on collagen-I (Type I-P, Nitta gelatin)-coated glass-bottom dishes or Lab-Tek chamber slides in a complete growth medium (see below) and allowed to adhere overnight. The cells were rinsed with pre-warmed Ca²⁺- and Mg²⁺-containing PBS once and fixed in pre-warmed 4% fresh PFA / PBS for 15 min, washed in PBS, and then permeabilized in 0.2% Triton X-100 in PBS for 5 min when necessary. The cells were incubated with blocking reagent (DAKO #X0909) for 10 min to inhibit nonspecific protein binding. For some experiments, the cells were alternatively fixed and permeabilized by immersion in acetone or methanol at –20 °C for 10 min. After blocking, cells were incubated with primary antibodies for 2 h at room temperature or overnight at 4 °C or with Alexa594-conjugated phalloidin (Molecular Probe #A-12381, 1:200). Then the cells were incubated for 1 h with goat AlexaFlour 488 or 594-conjugated secondary antibodies (1:1000) in PBS. In immunostaining of active GTP-RhoA, HUVEC were serum-starved in M199 medium including 0.5% fatty acid-free bovine serum albumin (BSA) for overnight and were stimulated with VEGF-A₁₆₅ (50 ng ml⁻¹) or EBM2 complete growth medium for 30 min and underwent double immunofluorescent staining by using active RhoA-specific antibody (for GTP-RhoA, NewEast Biosciences, #26904, 1:400), which is produced against GTPγS-bound RhoA antigen, and Alexa594-conjugated phalloidin (for F-actin) as described in above method. Where appropriate, cells were counterstained with 4', 6-diamidino-2-phenyliindole (DAPI, Molecular Probe, 300 nM) for 5 min. The cells were mounted on Prolong Gold (Molecular Probe) as an anti-photobleaching

agent and examined using an inverted fluorescence microscope (Olympus IX70) under a PlanApo $\times 40$ /NA0.95 objective, a confocal laser-scanning microscope (Zeiss Axiovert 200M with LSM5 Pascal) equipped with a $\times 63$ /NA1.4 PlanApo oil-immersion objective. For quantification of the amount of positive pixels, the positive area in stained images in each frame was calculated using Image J software. Quantifications represent at least three independent experiments with > 50 cells per experiment. Adobe Photoshop was used to adjust image levels and process image overlays.

Detection of LacZ by X-gal staining and immunostaining. For 5-bromo-4-chloro-3-indolyl- β -D-galactoside (X-gal) staining, whole embryos or tissues were dissected from E16.5–E18.5 embryos, fixed in X-gal fixative solution (0.25% glutaraldehyde, 5 mM EGTA, 2 mM MgCl_2 , in PBS) at room temperature for 30 min, and then washed in wash buffer (2 mM MgCl_2 , 0.02% NP-40 in PBS) for 10 min (3 times). Samples were stained in X-gal staining solution (1 mg ml^{-1} X-gal, 5 mM potassium ferricyanide, 5 mM potassium ferrocyanide in wash buffer) at 37 °C until desired staining level had been achieved. Alternatively, LacZ-specific antibody (MP Cappel #59761, 1:400) was used for multicolor-immunofluorescence staining, as described previously⁵⁶. Samples were imaged on a Leica MZ16F stereomicroscope (Whole-mount tissue) or a Zeiss Axiovert 200M microscopy with LSM5 Pascal confocal laser-scanning unit using Image Browser software (Carl Zeiss).

Postnatal retinal angiogenesis model. Eyes were dissected from neonatal mice (mutants or respective control littermates) and fixed in 4% PFA for 2 h at room temperature. Flat-mount Isolectin B4 staining of retinas was performed as described in *Whole-mount staining* section. The spreading of the retinal vasculature along the vitreal surface was quantified by flat-mounting the retina and analysis using Image-J software. The number of branch points and filopodial bursts in arterial zones per unit area in flat-mount retina was counted from randomly defined 15–20 microscopic fields from 5–8 retinas per group for each genotype. The values were normalized by field size. For labeling of proliferating cells in the retina, 300 μg of 5-bromo-2' deoxyuridine in 100 μl PBS (BrdU, BD) per pup was *i.p.* injected 2 h before sacrifice. Following isolectin-B4 staining, retinas were stained with BrdU-specific antibody (1:100, BD).

Post-ischemic hindlimb angiogenesis model. Male *Pik3c2a*^{iAEC} mice and littermates (C57BL/6 background) were subjected to surgical procedures to achieve unilateral hindlimb ischemia, as described previously⁵⁷. In brief, the femoral artery was exposed and ligated with 8–0 silk, and the whole length of the femoral artery was excised. The blood flow of the ischemic (left) and contralateral non-ischemic (right) hindlimbs was measured with a laser Doppler blood flow (LDBF) analyzer (Moor Instruments) before and after operation. The stored data were analyzed to quantify the mean LDBF per unit two-dimensional area on the en-face image of each entire hindlimb in mice in the supine position, which was determined by the software provided by the manufacturer (Moor Instruments). For each animal, the values were expressed as the ratio of LDBF values in the ischemic (left)/nonischemic control (right) limb at a given time point.

Tumor angiogenesis model. LLC cells (1×10^6) or B16-BL6 melanoma cells (5×10^5) were subcutaneously implanted in the dorsal back of 8–10 week old male *Pik3c2a*^{Δ^{EC}} and control littermates (C57BL/6 background)⁵⁸. Tumor volumes was calculated by the formula $V = (LW^2)/2$, where *L* and *W* denote the longer and shorter diameter, respectively.

PAF-induced anaphylaxis model. To trigger anaphylactic shock, 10–12 week old male *Pik3c2a*^{+/-} or littermate wild-type mice received *i.v.* injection of platelet-activating factor (PAF) (12 or 20 $\mu\text{g kg}^{-1}$ in 100 μl saline) via the tail vein, and survival was followed. In separate mice, 15 min after infusion, blood samples were obtained from the right ventricle to determine hematocrit. To assess vascular leakage in lung, 100 μl of a 1% solution of Evans blue dye in saline was injected into the tail vein together with PAF. 15 min later, mice were perfused with saline via the right ventricle to remove intravascular Evans blue dye. The lungs were excised and extracted in 1ml of formamide at 55 °C overnight. Evans blue content was determined by the equation; $\text{OD}_{620}(\text{corrected}) = \text{OD}_{620} - (1.426 \times \text{OD}_{740} + 0.03)$.

Angiotensin II infusion-aortic aneurysm model. An osmotic minipump (Alzet, model 1002) containing Ang II (1.0 mg kg^{-1} per day, Calbiochem) were implanted in the midscapular region in male *Pik3c2a* mutant and WT littermates. Mice were euthanized at day 14 after minipump implantation and aortic tissue was removed. The extent of aneurysms was graded according to the following criteria⁵⁹. Grade 1: remodeled tissue in suprarenal region frequently containing thrombus, Grade 2: pronounced bulbous form of Grade 1 containing thrombus, Grade 3: multiple aneurysms containing thrombus, Ruptured: ruptured aortic aneurysm. Both cryostat and paraffin-embedded aortic sections were used for characterization of aneurysmal lesions. Elastin was visualized using Elastica van Gieson (EVG) staining. Fibrosis was evaluated using Azan staining. Infiltrating macrophages were detected using Mac3-specific antibody (BD, 1:400) immunostaining. Miles assay and gelatin zymography were performed as described below.

Live-cell imaging and FRET analysis. Cells that had been transfected with the expression vectors for GFP-C2 α , GFP/mRFP-2 \times FYVE, and VE-cadherin-GFP/mRFP were plated on collagen-coated glass-bottomed dishes (MatTek, #P35G-1.5-20-C) or LabTek chamber slides (Thermo Scientific, #177402), and allowed to adhere for 16 h before imaging. Cells on a heated stage (37 °C, Tokai-Hit) were observed under a custom confocal microscope based on an inverted IX70 microscope (Olympus) equipped with an UPLSAPO $\times 60/\text{NA}1.35$ -oil or $\times 40/0.95$ -oil objective, confocal laser unit (CSU10, Yokogawa), EM-CCD digital camera (iXon, Andor) and Light engine (Lumencor, Inc) for 3D time-lapse (4D) confocal imaging at a rate of 2 frames per sec. The acquisition and process were controlled by iQ software (Andor).

For FRET analysis, HUVEC were transfected with the pRaichu-RhoA probe using an Amaxa Nucleofector system (Lonza), and imaged using a custom confocal microscope sytem configured with a

CFP and YFP filter set (Di01-T445/515/561-13×15×0.5, Semrock). Pseudo-grayscale ratio images were generated from images from CFP and FRET channels using Andor iQ software.

Cell proliferation, migration, adhesion, apoptosis and tube-formation assay. Cell proliferation was analyzed by MTS (3-(4,5-dimethylthiazol-2-yl)-5-(3-carboxymethoxyphenyl)-2-(4-sulfophenyl)-2H-tetrazolium, inner salt) assay kit (Promega) according to the manufacturer's instructions. For modified Boyden chamber cell migration assay, siRNA-transfected HUVEC (5×10^4 cells per well) resuspended in M199 medium (Gibco) containing 0.25% fatty-acid free BSA (Sigma-Aldrich) or adenovirus-infected MASM cells (2×10^4 cells per well) resuspended in serum-free DMEM, were placed in the upper chamber and allowed to migrate across collagen type I-coated polycarbonate filters (8 μm pore size, Neuro Probe) for 6 h toward the lower chamber with or without VEGF-A ($0.5\text{--}100 \text{ ng ml}^{-1}$) for HUVECs, and with or without PDGF-BB ($0.1\text{--}30 \text{ ng ml}^{-1}$) for MASM. The cells remaining on the upper surface of transwell membranes were removed and the cells that had migrated to the lower surface were methanol-fixed, stained with Diff-Quick (Sysmex), and counted in 5 random microscopic fields. To analyze cell adhesion to a collagen-covered surface, HUVEC that had been transfected with scrambled (control) or C2 α -siRNAs were seeded onto 96-well tissue culture plates coated with collagen type I and incubated in the presence of VEGF-A (30 ng ml^{-1}) for the indicated time periods. After washing with PBS three times to remove non-adherent cells, adherent cells were stained with Diff-Quick and quantified in triplicates with a microplate reader (Bio-Rad). For apoptosis assay, cells were immunostained with cleaved caspase-3-specific antibody according to the manufacturer's instructions (Cell Signaling). For tube formation assay, siRNA-transfected HUVEC (2.5×10^4 cells) in EBM2 containing 2% FBS with or without supplements were seeded onto 200 μl of growth factor-reduced Matrigel in a 24-well plate in the absence or presence of VEGF-A (30 ng ml^{-1}) and incubated for 12–16 h. Tube formation was quantified after 12–16 h by measuring the cumulative tube length and branching points number in five random microscopic fields by using ImageJ (NIH).

Pull-down assay of small G-protein activity. The pull-down assays for GTP-bound RhoA, Rac1 and Rap1 were performed as described previously⁵⁸. In brief, confluent HUVEC were stimulated and lysed with either the Rho extraction buffer (50 mM Tris-HCl pH7.5, 500 mM NaCl, 10 mM MgCl₂, 1% Triton X-100, 0.5% sodium deoxycholate, 0.1% SDS, 10% glycerol, protease/phosphatase inhibitor cocktail (Roche)), the Rac extraction buffer (50 mM Tris-HCl pH7.5, 500 mM NaCl, 10 mM MgCl₂, 1% Triton X-100, 0.5% sodium deoxycholate, 0.1% SDS, 10% glycerol, protease inhibitor cocktail), or the Rap extraction buffer (20 mM Tris-HCl pH7.5, 100 mM NaCl, 10 mM MgCl₂, 1% NP-40, 1 mM EGTA, protease inhibitor cocktail). The lysates were cleared by centrifugation and the resultant supernatants were incubated for 60 min at 4 °C with glutathione-Sepharose 4B beads coupled to the Rho binding domain of Rhotekin for RhoA, PAK1-CRIB domain for Rac1, and Rap binding domain of Ral-GDI for Rap1. The beads were washed and bound proteins were solubilized by the addition of 30 μl of SDS-PAGE 2 \times Laemmli's loading

buffer, followed by separation on 15% SDS-PAGE gels and western blotting with RhoA (1:1,000)-, Rac1 (1:2,000)- and Rap1 (1:1,000)-specific antibodies, respectively.

***In vitro* transwell and *in vivo* Miles permeability assay.** C2 α - or scrambled siRNA-transfected HUVEC were seeded onto collagen-coated transwells with 0.4 μ m pore-size (Costar) and allowed to form a monolayer. Permeability was stimulated with VEGF-A₁₆₅ (50 ng ml⁻¹) or thrombin (0.5 U ml⁻¹) for 30 min, followed by addition of FITC-dextran (a final concentration of 1 mg ml⁻¹) (*Mr* = 42 kDa, Sigma-Aldrich) into the top chambers and then incubation for additional 30 min. The amount of FITC-dextran in the bottom chambers was determined by fluorometric analysis.

For *in vivo* permeability assay, 1.0% Evans blue dye in saline (100 μ l) was *i.v.* injected into the tail vein of *Pik3c2a*^{+/+} and *Pik3c2a*^{+/-} mice, and allowed to circulate for 20 min. Recombinant human VEGF-A₁₆₅ (100 ng ml⁻¹, 100 μ l, PeproTech) or PBS was injected intradermally into the pre-shaved back skin. After 20 min, the mice were sacrificed, and the area of skin that included the entire injection site was removed. For Ang II-infusion model, 100 μ l of a 1% solution of Evans blue dye in saline was injected into the tail vein of male *Pik3c2a*^{+/-} or *Pik3c2a*^{+/+} littermate that received Ang II infusion for 14 days beforehand (1.0 mg kg⁻¹ per day). 30 min later, mice were perfused with saline via the right ventricle to remove intravascular Evans blue dye, and heart and aorta tissues were excised. Evans blue dye was extracted from the tissues by incubation with formamide overnight at 55 °C, and Evans blue content was determined spectrophotometrically as described above.

Metabolic cell labeling, lipid extraction and phosphoinositide measurement. The amounts of cellular phosphoinositides were determined as described previously⁶⁰. In brief, MEF cells were labeled for 48 h with 10 μ Ci ml⁻¹ [³H]-myo-inositol (Amersham Biosciences) in inositol-free DMEM containing 10% FBS. Labeling was quenched and lipids were extracted as described⁶⁰. Dried lipids were deacylated and analyzed by HPLC using a Partisphere SAX column (Whatman). Radioactivity was measured in 0.5 ml fractions using a liquid scintillation counter.

Statistical analysis. Unless otherwise noted, data are presented as means \pm SEM and were analyzed using Prism 5 software (GraphPad Software Inc). Paired data were compared by two-tailed Student's *t*-test or Mann-Whitney nonparametric *U*-test. Comparisons between multiple groups were analyzed by one- or two-way ANOVA with a subsequent post-hoc test. Results with *P* < 0.05 were considered statistically significant. The presented data represent at least three independent experiments.

Additional methods. Detailed methodology is described in **the online Supplementary Methods**.

52. Sorensen, I., Adams, R.H. & Gossler, A. Dll1-mediated Notch activation regulates endothelial

- identity in mouse fetal arteries. *Blood* **113**, 5680–5688 (2009).
53. Bazigou, E. *et al.* Integrin- $\alpha 9$ is required for fibronectin matrix assembly during lymphatic valve morphogenesis. *Dev Cell* **17**, 175–186 (2009).
 54. Takakura, N. *et al.* Critical role of the TIE2 endothelial cell receptor in the development of definitive hematopoiesis. *Immunity* **9**, 677–686 (1998).
 55. Benedito, R. *et al.* The Notch ligands Dll4 and Jagged1 have opposing effects on angiogenesis. *Cell* **137**, 1124–1135 (2009).
 56. Compagni A. *et al.* Control of skeletal patterning by ephrinB1-EphB interactions. *Dev. Cell* **5**, 217–230 (2003).
 57. Oyama, O. *et al.* The lysophospholipid mediator sphingosine-1-phosphate promotes angiogenesis in vivo in ischemic hindlimbs of mice. *Cardiovasc. Res.* **78**, 301–307 (2008).
 58. Du, W. *et al.* S1P₂, the G protein-coupled receptor for sphingosine-1-phosphate, negatively regulates tumor angiogenesis and tumor growth in vivo in mice. *Cancer Res.* **70**, 772–781 (2010).
 59. Deng, G.G. *et al.* Urokinase-Type Plasminogen Activator Plays a Critical Role in Angiotensin II-Induced Abdominal Aortic Aneurysm. *Circ. Res.* **92**, 510–517 (2003)
 60. Sasaki, T. *et al.* Function of PI3K γ in thymocyte development, T cell activation, and neutrophil migration. *Science.* **287**, 1040–1046 (2000).

Figure legends

Figure 1 Endothelial C2 α is necessary for developmental angiogenesis.

(a) Whole-mount CD31-specific immunohistochemical staining of the vasculatures in E11.5 wild-type and global *Pik3c2a*^{-/-} embryos. The magnified views show the brain (asterisk (left bottom)), dorsal aorta (red arrowhead (right bottom)) and intersomitic vessels (yellow arrowhead (right bottom)) in *Pik3c2a*^{-/-} embryo. Scale bar, 2 mm. (b) α SMA-specific immunohistochemical staining in cross-sections of dorsal aorta and heart from E11.5 wild-type and *Pik3c2a*^{-/-} embryos. Scale bar, 100 μ m. (c) Left three panels (top and bottom): gross views and HE staining of skin sections of E15.5 control and homozygous EC-specific C2 α -deletion mutant (*Pik3c2a* ^{Δ EC}) embryos (black arrowheads, normal dermal vessels; red arrowheads, dilated vessels and hemorrhage). Right three panels (top and bottom): whole-mount CD31 (red)- and α SMA (green)-specific, and VE-cadherin (red)- and NG2 (green)-specific double immunofluorescent staining of the skin sections in E15.5 control and *Pik3c2a* ^{Δ EC} embryos (white arrowheads in CD31 and α SMA staining, loosely attached α SMA⁺ SMCs; yellow and white arrowheads in VE-cadherin and NG2 staining, loosely attached and detached NG2⁺-pericytes, respectively). Arteriole (a) and venule (v) are indicated. Scale bar, 100 μ m. (d) Quantified data of vessel area and branch points. $n = 6$ mice per group. (e) CD31- and β -galactosidase (β Gal)-specific double immunofluorescent staining of brain sections in E15.5 control (*Pik3c2a*^{flox/flox}; *Rosa26R*) and EC-specific C2 α -deleted (*Pik3c2a*^{flox/flox}; *Tie2Cre*; *Rosa26R* (*Pik3c2a* ^{Δ EC}; *Rosa26R*)) embryos. Scale bar, 50 μ m.

Figure 2 C2 α is required for postnatal retinal angiogenesis.

(a) Western blot analysis of C2 α , p110 α , C2 β and Vps34 proteins in mouse lung EC (MLEC) and aortic smooth muscle cells (MASM) from 4-week old control (*Pik3c2a*^{flox/flox}) and *Pik3c2a*^{i Δ EC} mice with or without tamoxifen (Txf) administration as described in (b). (b) Diagram of experiments during early formation of retinal vasculature (P3–P6) in *Pik3c2a*^{i Δ EC}. Flat-mount Isolectin-B4 (IsoB4) staining of retinas from control (top; *Pik3c2a*^{flox/flox}) and tamoxifen (*i.p.* at P3)-inducible EC-specific C2 α deletion mutant mice (bottom; *Pik3c2a*^{i Δ EC}) at P6.

Yellow dots and arrowheads indicate filopodia and apoptotic cells, respectively. Scale bar, 100 μm . Vessel area and numbers of tip cells and filopodia per field were quantified (right). $n = 6\text{--}11$ mice per group. (c) Diagram of experiments during late development of retinal vasculature (P6–P9) in *Pik3c2a* ^{ΔEC} . The images of the sections at different levels in flat-mount IsoB4 staining of retinas from control and *Pik3c2a* ^{ΔEC} mice at P9 (left). Maximum intensity projection (MIP) images and x–z view of the retinal vasculature showing perpendicular sprouting (arrowheads) at P9 (right). Scale bar, 50 μm .

Figure 3 Tube-formation, cell migration and RhoA activation are impaired in C2 α -depleted HUVEC.

(a) Effects of siRNA-mediated PI3K knockdown on VEGF-A (20 ng ml⁻¹)-induced tube formation in serum/growth factor supplement-free medium. Scale bar, 200 μm . Quantification of total tube length (right). $n = 3$. (b) Effects of C2 α knockdown or deletion on VEGF-A-directed HUVEC migration and PDGF-BB-directed MASM migration. $n = 3$. (c) Effects of C2 α depletion on VEGF-A-induced signaling. (d) Quantification of VEGF-A-induced phosphorylation of MYPT1. (e) Effects of C2 α knockdown on VEGF-A-induced RhoA activation in HUVEC. The protein expression of C2 α and C2 β are shown on the top. (f) Quantified data of the results in (e). Data in (d) and (f) are shown as relative values of normalized band intensities. $n = 3$.

Figure 4 Endosomal transport and assembly of VE-cadherin and endosomal RhoA activation are impaired in C2 α -depleted EC.

(a) Fluorescent imaging of control HUVEC and C2 α -, p110 α -, or Vps34-depleted HUVEC transfected with mRFP-2xFYVE domain (PtdIns(3)P probe). Scale bar, 20 μm . Quantification of FYVE⁺-vesicle numbers per cell is shown (right). $n = 11\text{--}14$ cells. (b) Fluorescent imaging of VE-cadherin-GFP trafficking in control HUVEC, C2 α -, p110 α -, or Vps34-depleted HUVEC, and LacZ- or RhoA^{N19}-transfected HUVEC. Yellow arrowheads indicate VE-cadherin⁺ cell-cell contacts. Asterisks point to gaps between HUVEC. Scale bar, 20 μm . See also Supplementary movies 4 & 5. (c) Immunoprecipitation and western blot analysis

of the association of β -catenin (β -ctn) and p120-catenin (p120-ctn) with VE-cadherin (VEcad). Quantification of the results (right). $n = 3$. **(d–g)** HUVEC were transfected with the FRET probe expression vector pRaichu-RhoA. **(d)** VEGF-A-induced RhoA activation on the endosomes (yellow arrowheads) and the plasma membrane at cell-cell contacts (red arrowheads) in control and C2 α -depleted HUVEC. **(e)** VEGF-A-induced RhoA activation in HUVEC co-transfected with the expression vectors for Raichu-RhoA and mRFP-2xFYVE. Colocalization of endosomal FRET signals (yellow arrowheads (top)) with FYVE⁺-endosomes (white arrowheads (bottom)). Red arrowheads (top) indicate RhoA activation at cell-cell contacts. Scale bar, 20 μ m. **(f)** Quantification of endosomal RhoA activation in control and C2 α -depleted HUVEC. $n \geq 8$ cells. **(g)** Quantification of FYVE⁺-FRET signals in HUVEC. $n = 9–22$ cells. **(h)** Immunofluorescent staining of VEGFR2 (green) in mRFP-2xFYVE-cotransfected (#), control and C2 α -depleted HUVEC. Quantification of VEGFR2⁺- and FYVE⁺-HUVEC (right). $n = 8–20$ cells. Scale bar, 20 μ m.

Figure 5 Targeted deletion of endothelial C2 α decreases post-ischemic and tumor angiogenesis.

(a, b) Post-ischemic hindlimb angiogenesis. Ischemic/non-ischemic limb laser Doppler blood flow (LDBF) ratio in male 8-week old control and homozygous EC-specific C2 α deletion mutant (*Pik3c2a* ^{Δ EC}) mice **(a)**. $n = 13$ mice per group. CD31-specific immunofluorescent staining of sections of ischemic hindlimb muscle in control and *Pik3c2a* ^{Δ EC} mice **(b)**. Nuclei (blue) were stained with DAPI. Scale bar, 100 μ m. Quantification of CD31⁺ microvessel density on day 7 (right). $n \geq 20$ fields from at least 8 mice. **(c)** Representative LLC (top) and B16-BL6 tumors (bottom) in male 10-week old control and *Pik3c2a* ^{Δ EC} mice. Scale bar, 5 mm. Quantification of tumor weights and volumes (day 14) (right). $n \geq 7$ mice per group. **(d)** CD31-specific immunofluorescent staining of LLC tumor sections in control and *Pik3c2a* ^{Δ EC} mice. Scale bar, 200 μ m. Quantification of CD31⁺ microvessel density (right). $n = 7$ mice per group. **(e)** CD31- and NG2-specific double immunofluorescent staining of LLC tumor sections in control and *Pik3c2a* ^{Δ EC} mice. Yellow and white arrowheads indicate loose attachment and

detachment of pericytes, respectively, in *Pik3c2a*^{iΔEC} mice. Scale bar, 200 μm. Nuclei (blue) were stained with DAPI.

Figure 6 C2α disruption causes vascular hyperpermeability and dissecting aortic aneurysm formation *in vivo*.

(a) Effects of C2α depletion on VEGF-A-induced leak of FITC-dextran across HUVEC monolayers. *n* = 6. (b) Miles assay of VEGF-A-induced Evans blue leakage in skin of male 10-week old wild-type and *Pik3c2a*^{+/-} mice. Quantification of Evans blue leakage (right). *n* = 4–5 mice per group. (c) Survival of male 10-week old wild-type and *Pik3c2a*^{+/-} mice after PAF (12 or 20 μg kg⁻¹ *i.v.*)-induced anaphylaxis. Hematocrit after PAF (12 μg kg⁻¹ *i.v.*) challenge (right). *n* = 6 mice per group. (d) Extravasation of Evans blue dye in lung after PAF (12 μg kg⁻¹ *i.v.*) challenge. Scale bar, 5 mm. Quantification of Evans blue leakage (right). *n* = 3–6 mice per group. (e) Extravasation of Evans blue dye in aorta and heart of male 10-week old mice receiving chronic infusion of Ang II (1.0 mg kg⁻¹ per day for 2 weeks). *n* = 3–5 mice per group. (f) *En face* confocal microscopic views of VE-cadherin-specific immunofluorescent staining of aorta from male 10-week old mice given Ang II infusion. Scale bar, 50 μm. (g) Aneurysm formation of C2α mutant mice given AngII infusion. Gross view of aortic aneurysms (red arrowheads) (left top). Scale bar, 1 mm. Incidence of aortic aneurysms in control, *Pik3c2a*^{+/-} and *Pik3c2a*^{iΔEC} mice (right top). The severity of aneurysms was graded as described in the Online Methods section. Azan-stained sections of dissecting aortic aneurysm in *Pik3c2a*^{+/-} mice (bottom). Scale bar, 500 μm. PL, pseudo-lumen; Red arrowhead, adventitia; black arrow, internal elastic lamina (IEL); yellow arrow, external elastic lamina (EEL); asterisk, true lumen of aorta. (h) Survival of male 8–10 week old mice given Ang II infusion. (i) Matrix metalloproteinase (MMP)-2/9 activities are increased in aorta of male 10-week old mice given Ang II infusion. Quantification of MMP-2/9 activities. *n* = 6 mice per group. (j) Mac3-specific immunohistochemical staining of the aortic wall of male 10-week old mice given Ang II infusion. Red arrowheads, infiltrating macrophages; black arrow, internal elastic lamina (IEL); yellow arrow, external elastic lamina (EEL). Scale bar, 200 μm. In (c), (g), and (h), mouse numbers are

shown in parentheses.

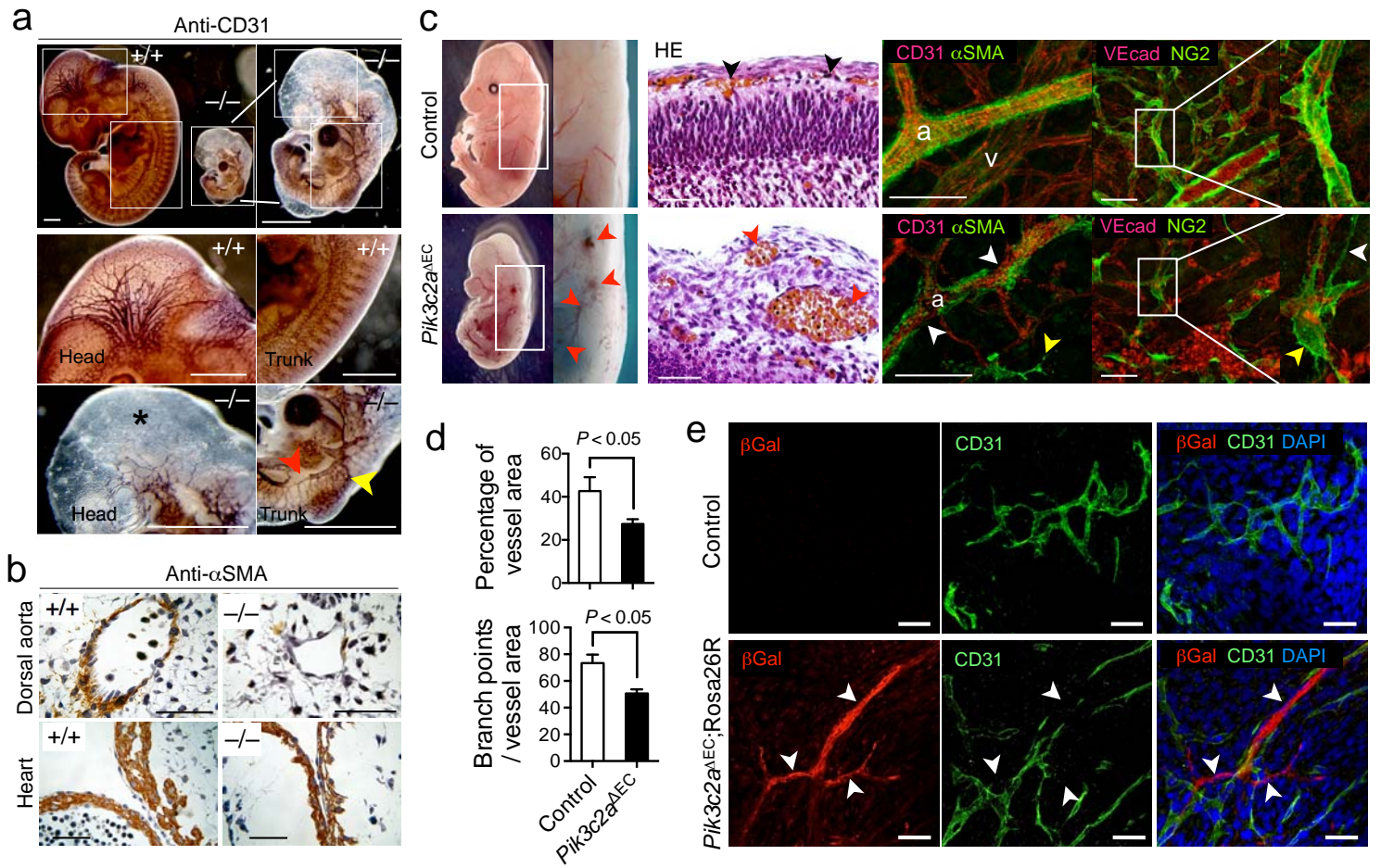


Fig. 1 K. Yoshioka *et al.*

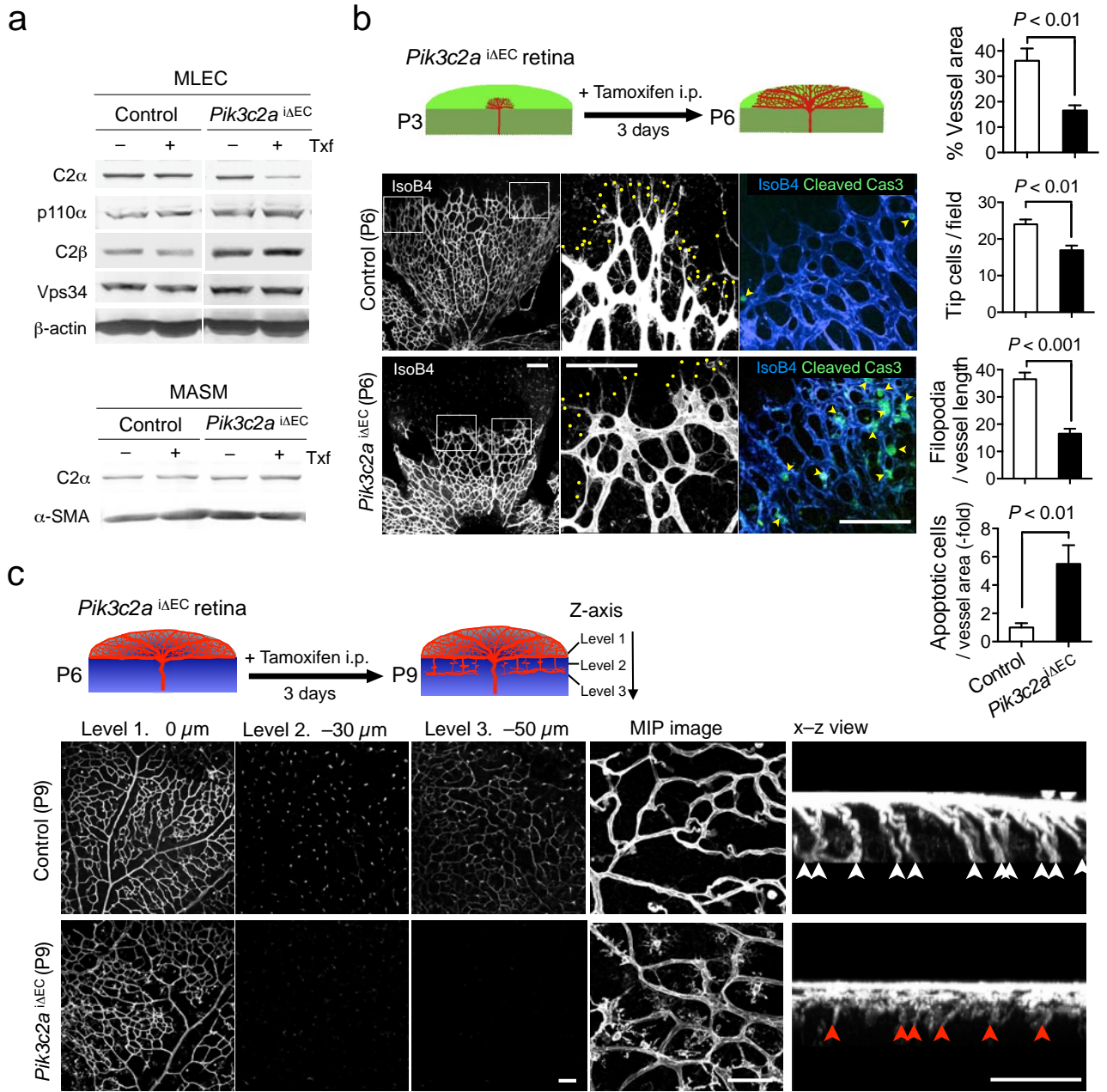


Fig. 2 K. Yoshioka *et al.*

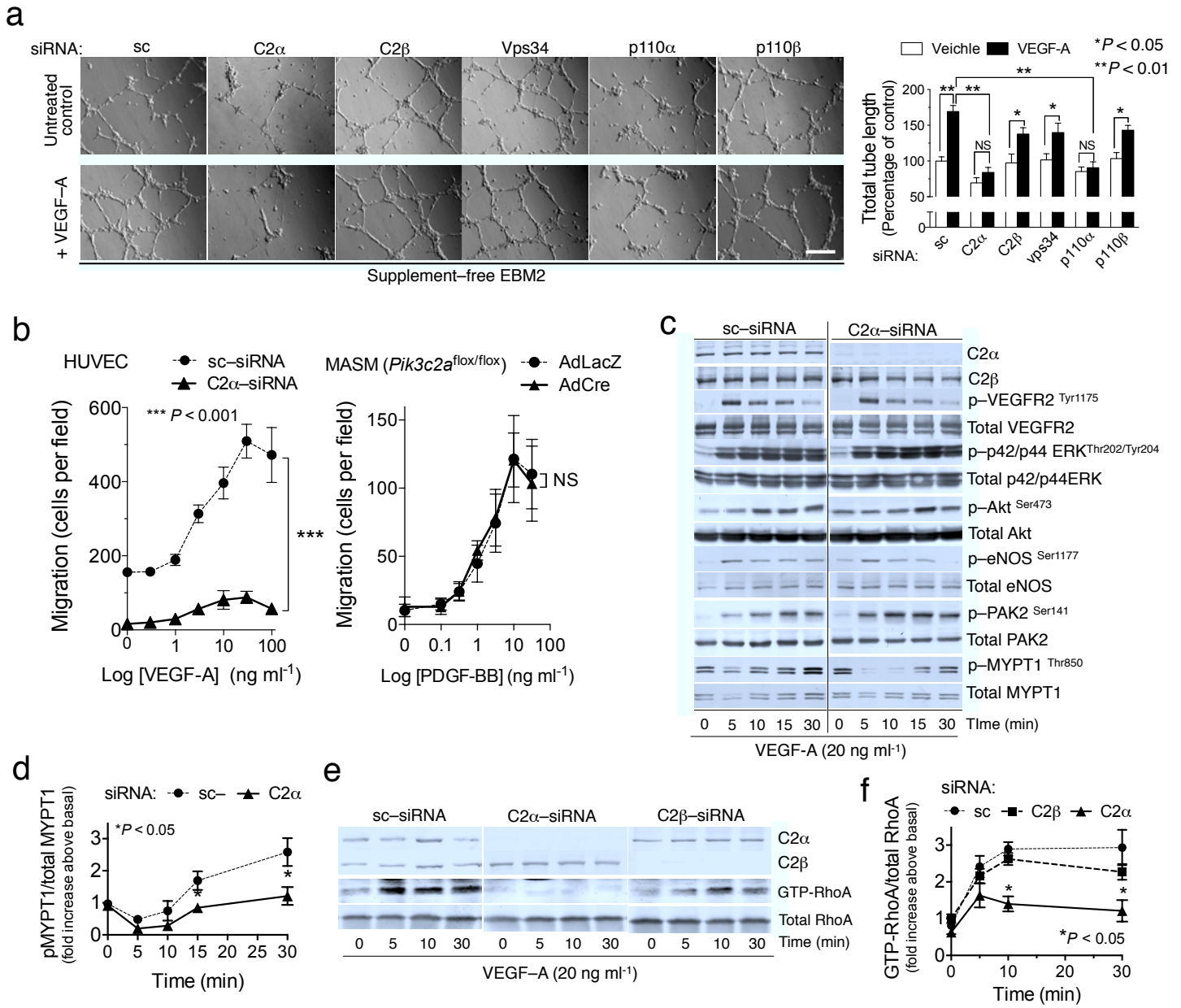


Fig. 3 K. Yoshioka *et al.*

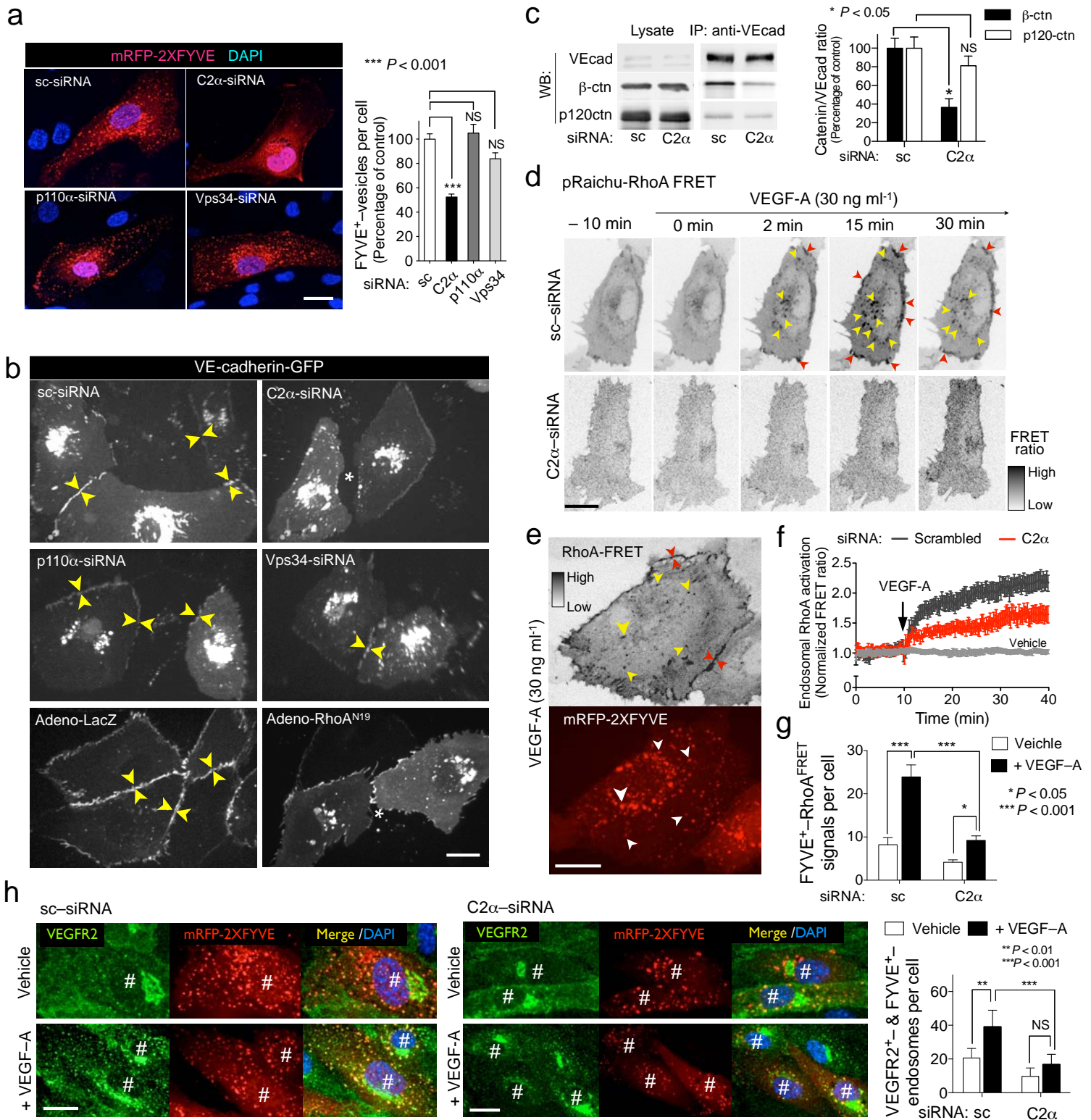


Fig. 4 K. Yoshioka *et al.*

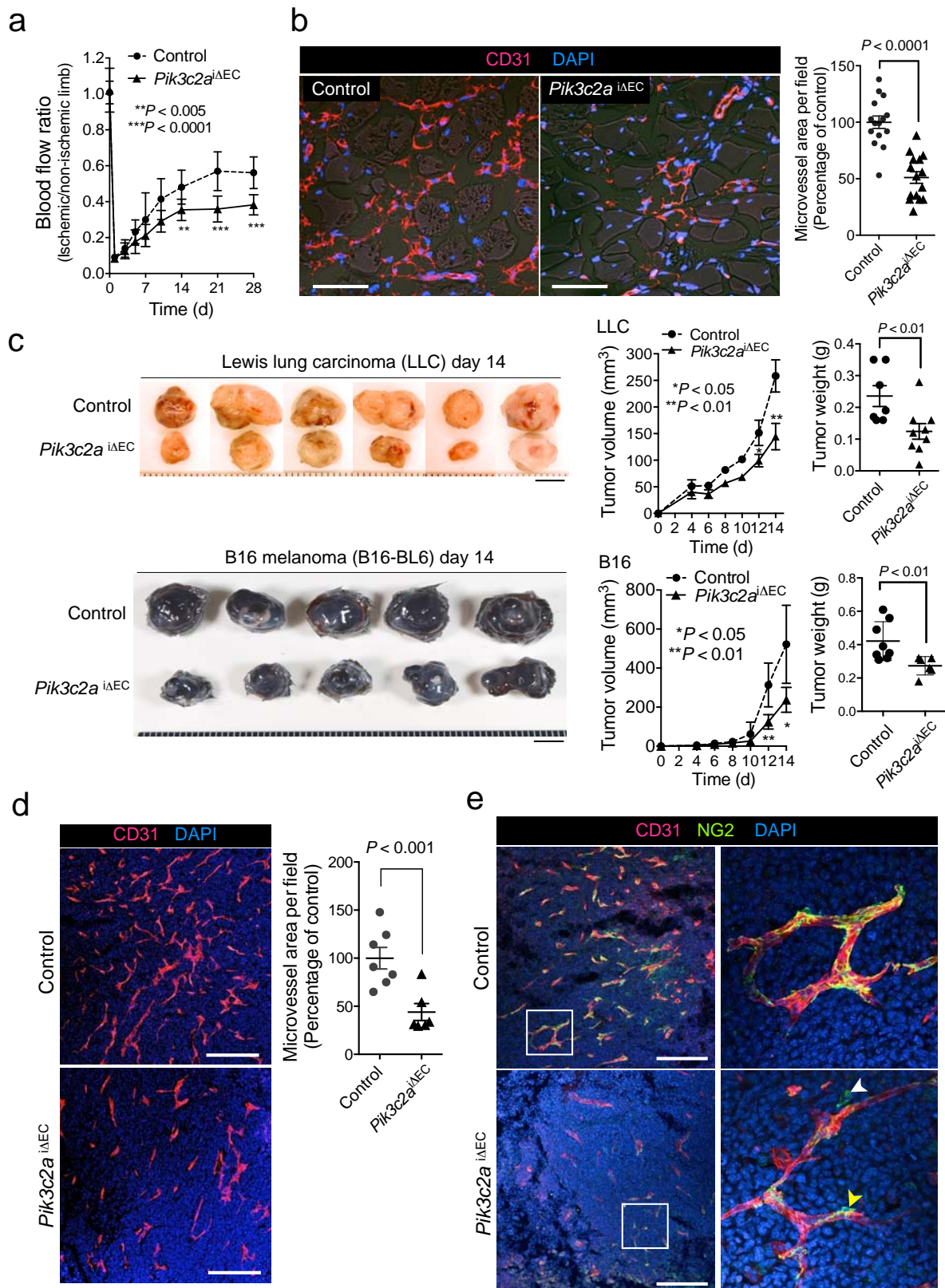


Fig. 5 K. Yoshioka *et al.*

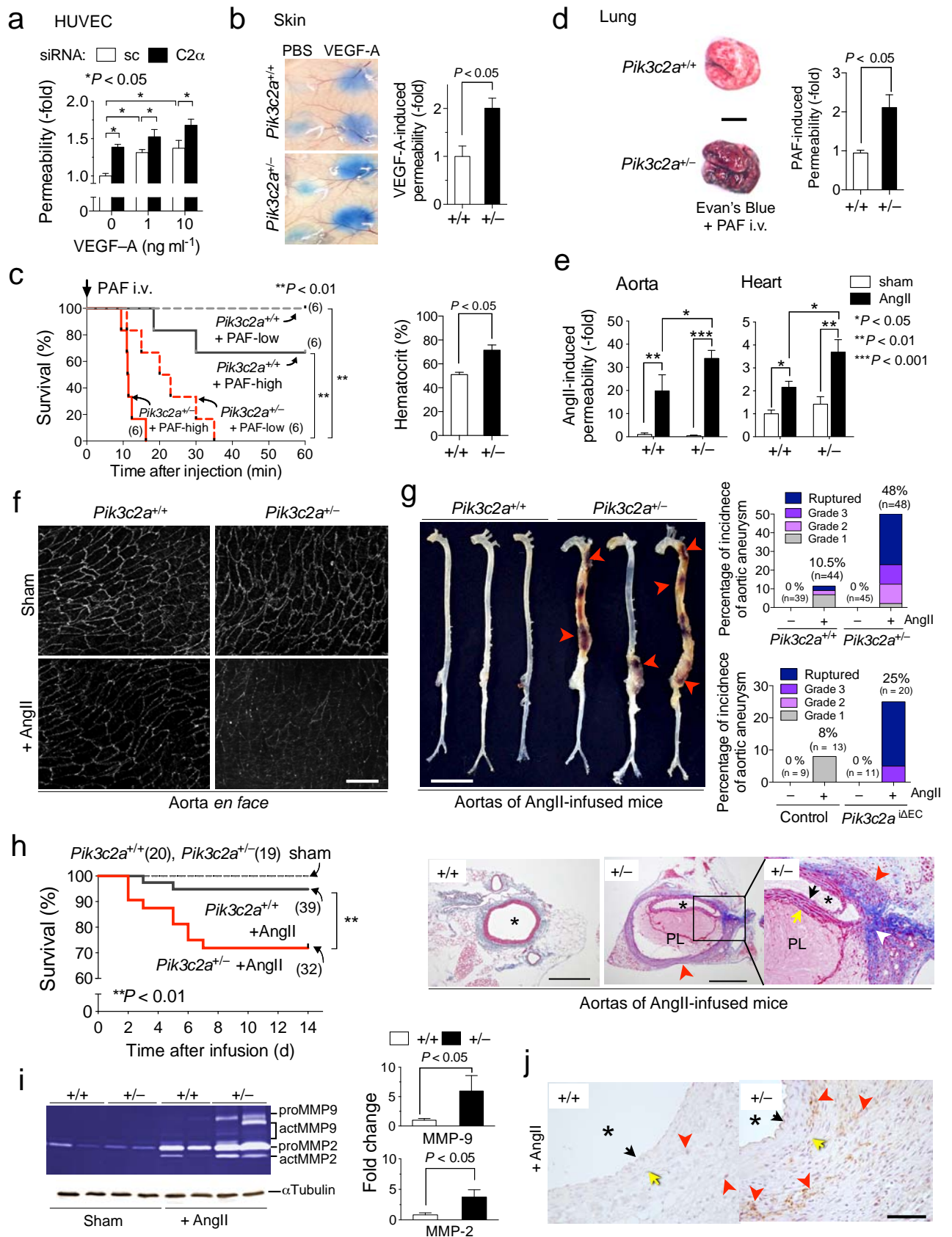


Fig. 6 K. Yoshioka *et al.*